Chapter III

Raman and photoluminescence studies of WS_2/C-dot nanohybrid systems

Typically, the C-dots are a new class of carbon nanomaterials with a size of less than 10 nm. As compared to the traditional semiconductors, carbon dots (C-dots) are superior in terms of solubility, chemical inertness, biocompatibility and photo-emission property [1-3]. Moreover, the C-dots are capable of exhibiting both size and excitation wavelength dependent photoluminescence (PL) property [1]. In contrast to the processing of 2D WS_2 nanosheets by a facile, hydrothermal route followed by ultrasonication, the C-dots were obtained via a green route, considering orange juice as the source of carbon. The mechanism of formation of C-dots from orange juice involves hydrothermal carbonisation of the major constituents, such as, sucrose, glucose, fructose, citric acid and ascorbic acid [5]. In this chapter, we highlight physical properties of WS_2/C-dot hybrid nanosystems, emphasizing light-matter interaction and particularly, probing Raman active modes and excitation dependent photoluminescence properties.

3.1 Principles of light scattering and light emission processes

Light scattering is an optical phenomenon caused by the interaction of light with a particle in a solution [6]. When light strikes a particle in a solution photons are absorbed by the particle and re-emits in all direction. This phenomenon is called scattering [6]. The majority of the photons are scattered elastically i.e. the frequency of the emitted photons are same as that of the incident light. This type of scattering process is called Rayleigh scattering [7]. However, a small fraction of light (one out of 10^7 photons) scatters with frequency lower or higher than the frequency of the incident photons. This type of inelastic scattering is called Raman scattering [7]. Raman scattering occurs with a change in the vibrational, rotational and electronic energy of a molecule. The difference in energy between the incident photons and inelastically scattered photons is equal to the energy of vibration of the scattered molecule.

When light interacts with the molecules, it leads to molecular deformation and a dipole moment is induced. Due to the molecular deformation the molecule starts vibrating with a characteristic frequency υ_m. If the frequency of the incident light is υ_0, and it is seen that most of the light get scattered with the same frequency of

υ_0, it is called as, Rayleigh scattering. A small fraction of light is found to scatter with a frequency υ_0-υ_m, which is called Stokes Raman frequency [8]. And a very small fraction of light is found to scatter with a frequency of $\upsilon_0 + \upsilon_m$, called anti-Stokes frequency [8].

The Raman shift $\Delta\upsilon$ doesn't depend upon the frequency of the incident light but it is the characteristic of the material causing the Raman effect.

3.2 Raman active modes in the WS_2/C-dot nanohybrid system

Raman spectroscopy is an important, yet versatile tool to characterise Raman active vibrational modes in a given specimen. The, extensive Raman analysis is capable of providing information as regards, number of layers, nature of defects, doping levels, microstrain and other useful details [9]. Fig. 3.1 (a) represents a set of Raman spectra of the synthesized nano-WS_2 system acquired at an excitation wavelength, λ_{ex} ~785 nm. The WS_2 nanosheets showed two major Raman active vibronic bands, E^1_{2g} and A_{1g} modes, which are found to be located at ~350 cm^{-1} and 420.3 cm^{-1}; respectively [10]. These modes essentially correspond to the in-plane optical mode and out-of plane vibrational modes of the sulfur atoms within the nano-system [10]. For clarity, a zoomed in version of these peaks are

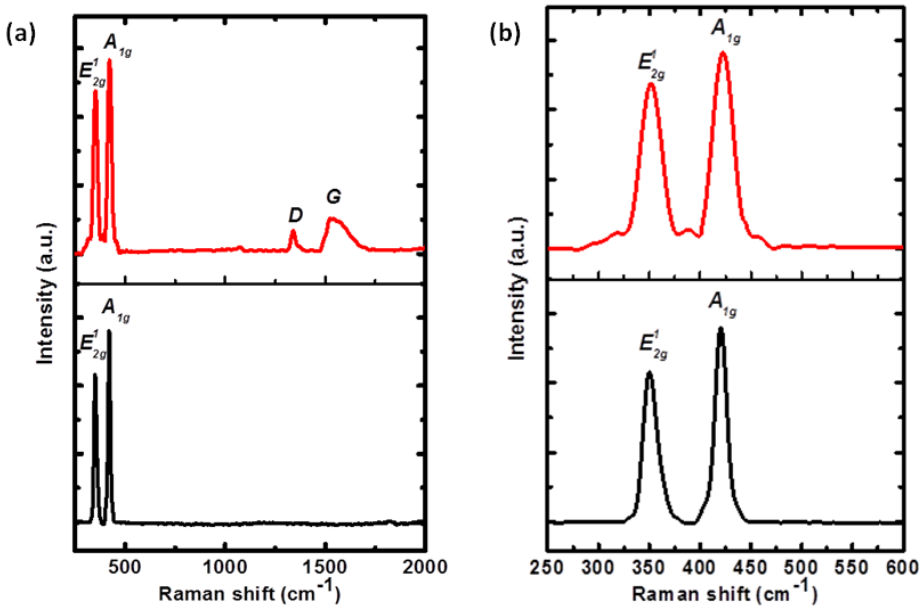

Figure 3.1: Raman spectra of the WS_2 nanosheet and WS_2/C-dot nanohybrid systems. The magnified views of the E^1_{2g} and A_{1g} modes are highlighted in (b).

depicted in Fig. 3.1 (b). Relative to WS_2 only nano-system, the E^1_{2g} and A_{1g} Raman active modes of the WS_2/C-dot nanohybrid system are shifted marginally toward the higher frequency side by approximately, 2.83 cm^{-1} and 1.40 cm^{-1}, respectively.

Moreover, the E^1_{2g} to A_{1g} intensity ratio of the nanohybrid system, experienced a marginal improvement from a value of 0.70 to a value of 0.79. Also, the full width at half maxima (FWHM) of the modes get improved substantially (Table 3.1). The overall feature is ascribed to the strong interaction between the C-dots and the WS_2 nanosheets, which can strengthen both the in-plane and out-of-plane effective restoring forces acting on them [11]. Furthermore, the emergence of two additional peaks located at ~1335.7 cm^{-1} and 1531 cm^{-1} are assigned to the *D* and *G* bands of the graphitic content [12]. While the *D* band corresponds to defects existing in the graphitic carbon material, the G band is linked to the sp^2 carbon atoms in the graphitic layers [13]. Since the *G* band appears due to the stretching of the *C-C* bonds in the sp^2 bonded material, the asymmetric nature might have arisen due to the presence of unsaturated bonds at the adjoining interface of the WS_2 and the C dots. Upon de-convolution (not shown), the *G*-band was seen to offer three superimposed peak maxima, positioned at ~1519.8 cm^{-1}, 1551.7 cm^{-1} and 1595.9 cm^{-1}.

Table 3.1: Raman spectra analysis of WS_2 and WS_2/C-dot nanoscale system

Sample	Raman modes	FWHM (cm^{-1}) E^1_{2g}; A_{1g}	Intensity ratio (E^1_{2g}/A_{1g})
WS_2 nanosheet	E^1_{2g} and A_{1g}	16.45; 13.59	0.70
WS_2/C-dot nanohybrid	E^1_{2g} and A_{1g}; *D* and *G* (graphitic)	23.54; 22.62	0.79

3.3 Ordinary and excitation dependent photoluminescence

Photoluminescence is an optical phenomenon shown by many of the materials, particularly which possess a band gap. When a material is excited by an electromagnetic radiation (hυ), the electrons are excited to the conduction band leaving the holes in the valence band. The electrons drop back to the valence band and recombine with the holes by emitting photons, whose energy (hυ′), is generally less than the excitation energy (hυ). The time interval between the absorption and emission of photons may vary from femtoseconds to milliseconds. Accordingly they are called as, fluorescence and phosphorescence; respectively [14]. In case of semiconductors, the most common radiative transition occurs between the states of the conduction band and the valence band. The near-band-edge emission is the most common type of radiative emission. However, the radiative transitions in semiconductors may also include transitions accompanied by localized defects and impurity levels [15].

In case of most of the materials the emission energy do not depend on the absorption energy, i.e. the material will show its PL peak at a particular wavelength which does not vary with the excitation wavelength. Such type of photoluminescence process is called ordinary or excitation independent photoluminescence process [16]. Most of the semiconductors like ZnO, ZnS, TiO_2 etc. show excitation independent photoluminescence [17, 18]. The size dependent luminescence feature (due to quantum confinement) is also accommodated in this category.

On the other hand, in case of some other materials, like graphene and carbon dots (C-dot) the emission wavelength was found to vary with the excitation lines. Such type of unconventional photoluminescence processes are called as, excitation dependent photoluminescence [19]. Without varying size, the PL properties of these materials can be tuned by varying the excitation wavelength. The origin of ordinary and excitation dependent PL processes are distinctly different; with latter may arise due to manifestation of one or more processes. Multicolour emission capabilities of the materials exhibiting such PL processes have become very useful from the application point of views [19].

3.4 Excitation dependent luminescence feature of WS_2/C-dot nanohybrid

First we discuss about optical absorption responses prior to luminescence ones. The UV visible optical absorption spectra of both WS_2 nanosheets and 2D WS_2/C-dot nanohybrid samples are depicted in Fig. 3.2 (a). It may be noted that, C-dots were not prepared separately rather, processed in a precursor containing WS_2. Accordingly, absorption and photoluminescence responses of the hybrid WS_2/C-dot nanosystem are compared with the WS_2 only system. The absorption band at ~ 632 nm corresponds to the *d–d* type transitions of the WS_2 at the center of the Brillouin zone [20]. The absorption band at ~525 nm is ascribed to the transitions arising from the spin-splitted valence band to the conduction band [21], and the band located at ~450 nm may arise from the localized density of states (DOS) existing between the valence and conduction bands [21]. The absorption spectrum of the WS_2/C-dot hybrid system, however, gave multiple peaks: ~ 270 nm, 295 nm, 450 nm, 520 nm and 630 nm. In fact, the C-dots are known to exhibit broad UV absorption at ~ 295 nm, which is the characteristic peak of carbon rich nanoparticles synthesized by way of carbonization of chitosan [22]. Fig. 3.2 (b) represents the corresponding PL spectra under an excitation wavelength of λ_{ex} = 360 nm. As can be noticed, the hybrid WS_2/C dot nanosystem gives a much improved luminescence response due to enriched radiative property introduced by the C-dots, behaving like fluorophore agents. Since the PL spectra of the WS_2 nanosheet and WS_2/C-dot hybrid systems share the similar line-shape, one can anticipate relevant surface interaction between the WS_2 nanosheets and the C-dots in the hybrid system. Moreover, the digital snap shots of the cuvette containing WS_2/C-dot nanohybrid specimen and captured under white and UV light illuminations, can be found in Fig. 3.2 (c). To be specific, the yellow coloured specimen under visible light turns blue under UV light exposure.

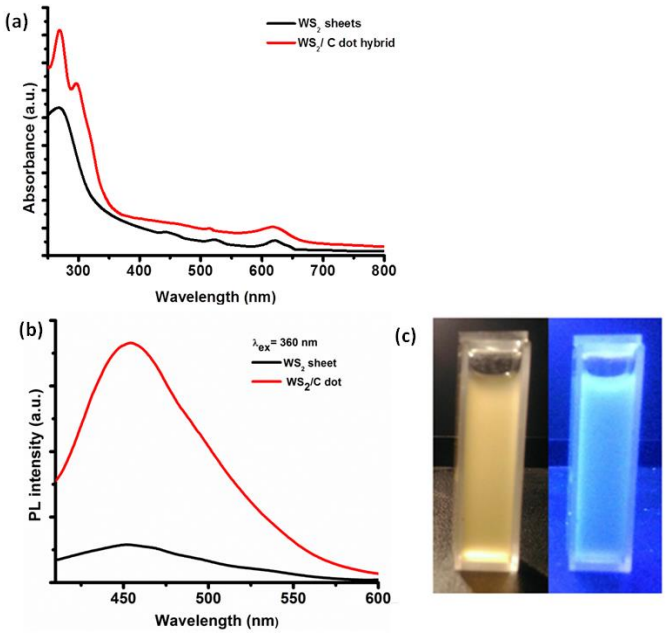

Fig. 3.2 A : (a) UV visible optical absorption and (b) PL emission spectra (λ_{ex} = 360 nm) of the synthesized WS_2/C -dot nanosystems. Digital photographs captured under visible and UV light exposure of the cuvette containing nanohybrid specimen, are shown in (c).

A series of excitation wavelength dependent PL spectra of the WS_2/C-dot hybrid system are shown in Fig. 3.2 (B) (a). When the excitation wavelength (λ_{ex}) is changed from 350 nm to 440 nm, the corresponding PL emission peaks (λ_{em}) get altered with the central maxima varying between ~450 nm (blue) and 531 nm (green). Moreover, we also noticed a small emission peak at ~714 nm corresponding to λ_{ex} = 560 nm, shown as inset in Fig. 3.2 (B) (a). As a general trend, with the increase in the excitation wavelength, the PL emission intensity first improves and then, gets weakened by substantial amount. However amount. However, the up-converted PL property of the C-dots, which is reported to be an important reason to improve the photocatalytic activity of such kind of hybrid cannot be ensured in this case [17]. On the other hand, the PL excitation spectra have been acquired keeping wavelength of emission fixed (Fig. 3.2 (B) (b)). Note the nature of curves with increasing wavelength of emissions.

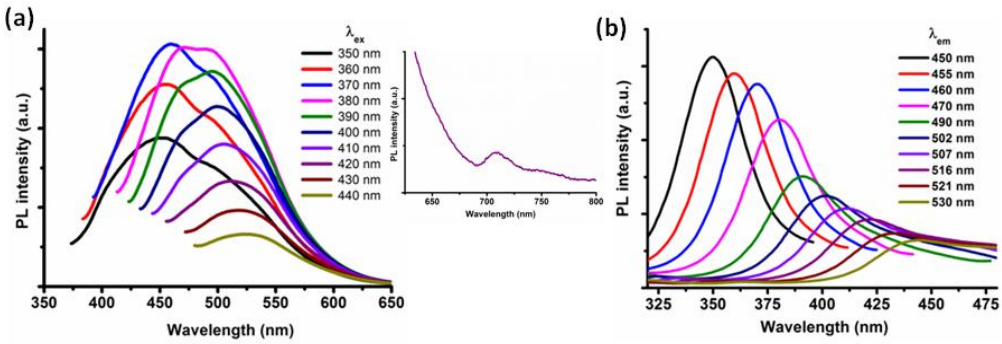

Figure 3.2 B: A series of (a) excitation dependent PL emission spectra and that of (b) PL excitation spectra of the WS_2/C-dot nanosystem. Since excitation at λ_{ex} = 560 nm gives a weak emission peak at λ_{em} = 714 nm, it is shown independently as figure inset of (a).

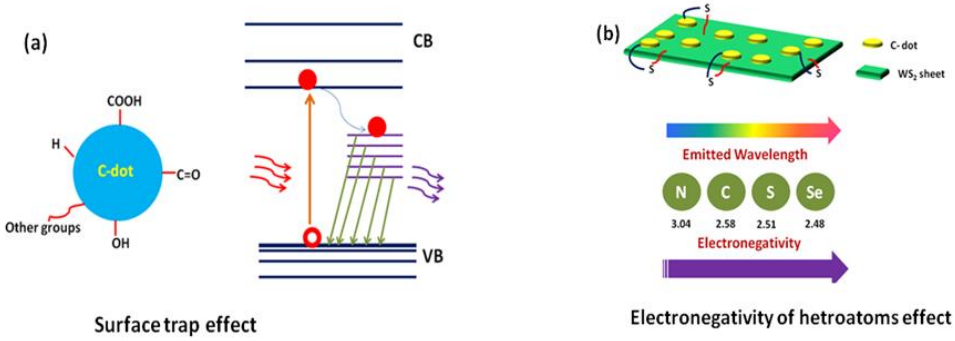

Figure 3.3: Schematic representation of the effects responsible for excitation dependent PL spectra.

At present, there is no clear cut mechanism available to justify the excitation dependent luminescence in layered systems. However, in graphene quantum dots and its derivatives, different groups have advocated excitation dependent luminescence as a consequence of quantum size effect, giant red-edge effect, surface trap and heteroatoms [23]. In our case, we expect the latter mechanisms to be mainly responsible for displaying excitation dependent PL features. The surface traps model essentially relies on adequate trap states due to the oxygen rich groups, such as, -COOH and OH available at the surface of the C- dots. The availability of continuous yet different localized defect states would account for the PL emission responses at different wavelengths [24–26]. On the other hand, electronegativity of heteroatom model suggests that, surface active groups and

heteroatoms may influence the PL response of the C-dots significantly. The fluorescence peak would experience redshifts when C-dots are doped with S or Se, which act as electron donors owing to their low electronegative character [24].

Since the WS_2 nanosheets are evolved with ample dangling bonds, when anchored with the C-dots, the latter might be crowded with free S-atoms at the interface. Consequently, C-dots would realize edge doping with S and can become responsible for the excitation dependent red shifting in the PL spectra [24, 27]. The schematic illustrations of surface-trap effect and electronegativity of heteroatoms are depicted in Fig. 3.3 (a, b). In order to substantiate excitation dependent response, fluorescence microscopy was also employed to exploit fluorescent nature of the synthesized WS_2/C-dot nanosystem, images being shown in Fig. 3.4 (a-d). Apparently, the images exhibited brown, blue, green and red impressions, when the nanohybrid specimen was excited with white, UV, blue and green light; respectively. Note the well dispersed bright spots in each case, which are believed to have arisen from the surface anchored C-dots spread over the WS_2 nanosheets.

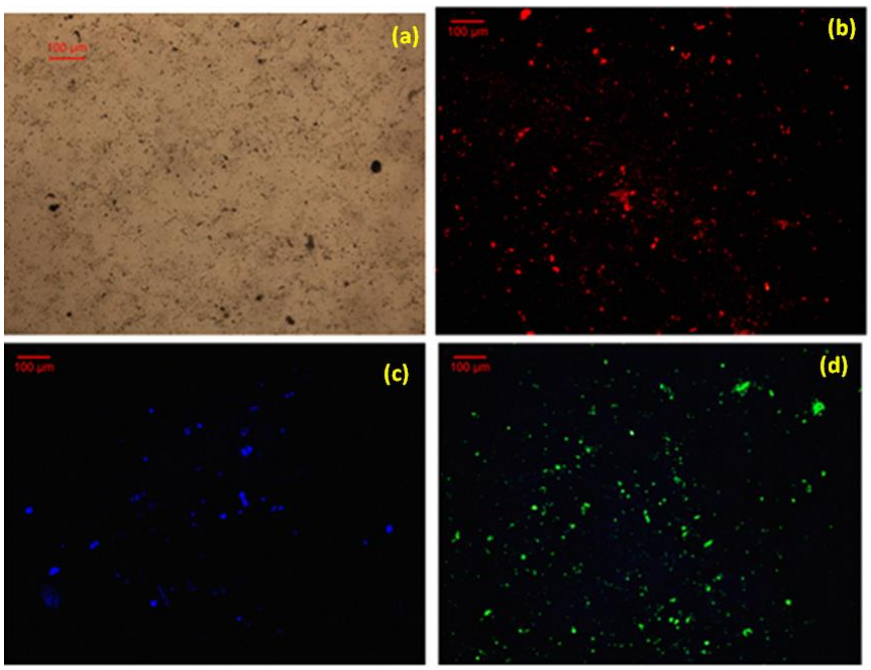

Figure 3.4: The fluorescence micrographs under different excitation source: for which (a) white, (b) UV, (c) blue, and (d) green band-pass filters have been used.

3.5 Conclusion

The synthesized WS_2/C-dot nanohybrids were found to exhibit excellent fluorescence property, which are highly tunable with the excitation wavelength. The PL spectra of the WS_2/C-dot hybrid system displayed an overall rise, because of the presence of the fluorophore like C-dots. The underlying mechanism for exhibition of excitation dependent PL and red-shifting response has been attributed to models related to surface traps and electronegativity of heteroatoms. Moreover, as compared to the WS_2 nanosheets, the Raman spectrum of the WS_2/C-dots hybrid nanosystem offered a marginal shifting of both the in-plane optic and out of plane vibronic modes, namely, E^1_{2g} and A_{1g}; toward lower frequency side along with the evolution of two additional peaks, assigned to the *D* and *G* bands of the graphitic system.

References

[1] Wang, Y., Hu, A. Carbon quantum dots: synthesis, properties and applications, *Journal of Material Chemistry C*, 2: 6921-6939, 2014.

[2] Zhang, Z., Zheng, T., Li, X., Xu, J., Zeng, H. Progress of carbon quantum dots in photocatalysis applications, Particle and Particle Systems Characterization, 33:457-472, 2016.

[3] Atabaev, T. S. Doped carbon dots for sensing and bioimaging applications: a mini review, *Nanomaterials*, 8:342 (2018)

[4] Sahu, S., Behera, B., Maiti, T.K., Mohapatra, S. Simple one-step synthesis of highly luminescent carbon dots from orange juice: application as excellent bio-imaging agents, *Chemical Communications*, 48: 8835-8837, 2012.

[5] Marmer, D. J., Hurtubise, P. E. Nephelometric and turbidimetric immunoassay. *Immunoassay,* ISBN: 978-0-12-214730-2, Academic Press, pages 363–387, 1996.

[6] Bumbrah, G. S., Sharma, R. M. Raman spectroscopy–Basic principle, instrumentation and selected applications for the characterization of drugs of abuse. *Egyptian Journal of Forensic Sciences*, 6:209–215, 2016.

[7] Lewandowska, R., Liu, J. Raman Microscopy: Analysis of Nanomaterials. *Reference Module in Materials Science and Materials Engineering*, doi:10.1016/B978-0-12-803581-8.02593-5, 2016.

[8] Wang, F., Kinloch, I.A., Wolverson, D., Tenne, R., Zak, A., Connell, EoghanO', Bangert, U., Young, R. J. Strain-induced phonon shifts in tungsten disulfide nanoplatelets and nanotubes, *2D Materials*, 4: 015007, 2016.

[9] Atkin, P., Daeneke, T., Wang, Y., Carey, B.J., Berean, K.J., Clark, R.M., Ou, J.Z., Trinchi, A., Cole, I.S., Kalantar-zadeh, K. 2D WS_2/carbon dot hybrids with enhanced photocatalytic activity. *Journal of Material Chemistry A*, 4:13563, 2016.

[10] Huo, N., Wei, Z., Meng, X., Kang, J., Wu, F., Li, S.-S., Wei, S.-H., Li, J. Interlayer coupling and optoelectronic properties of ultrathin two-dimensional heterostructures based on graphene, MoS_2 and WS_2. *Journal of Material Chemistry C*, 3: 5467, 2015.

[11] Ding, H., Cheng, L.-W., Ma, Y.-Y. , Kong, J.-L. , Xiong, H.-M. Luminescent carbon quantum dots and their application in cell imaging, *New Journal of Chemistry*, 37:2515 -2520, 2013.

[12] Zhou, S., Chen, J., Gan, L., Zhang, Q., Zheng, Z., Li, H., Zhai, T. Scalable production of self-supported WS_2/CNFs by electrospinning as the anode for high-performance lithium-ion batteries. *Science Bulletin*, 61(3): 227 -235, 2016.

[13] Hayes, G.R., Deveaud, B. Is Luminescence from Quantum Wells Due to Excitons?. *Physica Status Solidi A*, 190(3): 637–640, 2002.

[14] Perkowitz, S., Nishizeki, T., Chiba, N. *Optical Characterization of Semiconductors*. Academic Press, 1993.

[15] Wen, Z-H., Yin, X-B. Excitation-Independent Carbon Dots, from Photoluminescence Mechanism to Single-Color Application. *RSC Advances*, 6:27829-27835, 2016.

[16] Moloto, N., Mpelane, S., Sikhwivhilu, L. M., Ray, S. S. Optical and Morphological Properties of ZnO- and TiO2-Derived Nanostructures

Synthesized via a Microwave-Assisted Hydrothermal Method, *International Journal of Photoenergy*, Article ID 189069, 6 pages, 2012.

[17] Chandrakar, R.K., Baghel, R.N., Chandra, V.K., Chandra, B.P. Synthesis, characterization and photoluminescencestudies of undoped ZnS nanoparticles. *Superlattices and Microstructures*, 84:132–143, 2015.

[18] Wang, Y., Hu, A. Carbon quantum dots: synthesis, properties and Applications. *Journal of Material Chemistry C*, 2:6921-6939, 2014.

[19] Notley, S.M. High yield production of photoluminescent tungsten disulphide nanoparticles. *Journal of Colloid and Interface Science*, 396:160 - 164, 2013.

[20] Zhou, M., Zhang, Z., Huang, K., Shi, Z., Xie, R., Yanga, W. Colloidal preparation and electrocatalytic hydrogen production of MoS_2 and WS_2 nanosheets with controllable lateral sizes and layer numbers. *Nanoscale*, 8:15262, 2016.

[21] Yang, Y., Cui, J., Zheng, M., Hu, C., Tan, S., Xiao, Y., Yang, Q., Liu, Y. One-step synthesis of amino-functionalized fluorescent carbon nanoparticles by hydrothermal carbonization of chitosan. *Chemical Communications*, 48:380- 382, 2012.

[22] Li, H., He, X., Kang Z., Huang H., Liu Y., Liu J., Lian S., Tsang C.H.A., Yang X., Lee, S.-T. Water-soluble fluorescent carbon quantum dots and photocatalyst design. *Angewandte Chemie*, 49:4430- 4434, 2010.

[23] Gan, Z., Xu, H., Hao, Y., Mechanism for excitation-dependent photoluminescence from graphene quantum dots and other graphene oxide derivatives: consensus, debates and challenges. *Nanoscale*, 8:7794-7807, 2016.

[24] Lee, J., Kim, K., Park, W.I., Kim, B.H., Park, J.H., Kim, T.H., Bong, S., Kim, C.H., Chae, G.S., June, M., Hwang, Y., Jung, Y.S., Jeon, S., Uniform graphene quantum dots patterned from self-assembled silica nanodots. *Nano Letters*. 12:6078-6083, 2012.

[25] Xu, Q.F, Zhou, Q., Hua, Z., Xue, Q., Zhang, C.F., Yang, X.Y., Pan, D.Y., Xiao, M. Singleparticle spectroscopic measurements of fluorescent graphene quantum dots, *ACS Nano*, 7:10654-10661, 2013.

[26] Sun, J., Yang, S.W., Wang, Z.Y., Shen, H., Xu, T., Sun, L.T., Li, H., Chen, W.W., Jiang, X.Y., Ding, G.Q., Kang, Z.H., Xie, X.M., Jiang, M.H. Ultra-high quantum yield of graphene quantum dots: aromatic-nitrogen doping and photoluminescence mechanism, *Particle and Particle Systems Characterization*, 32:434-440, 2015.